Meteorology and Atmospheric Physics (2023) 135:11
https://doi.org/10.1007/s00703-022-00949-8

ORIGINAL PAPER

Comparison between warm-sector and frontal heavy rainfall events in South China and the objective classification of warm-sector heavy rainfall events

Yanan Fu[1,3] · Jianhua Sun[1,2,3] · Shenming Fu[4] · Yuanchun Zhang[1]

Received: 17 April 2022 / Accepted: 15 December 2022

Abstract
In this study, a total of 402 warm-sector heavy rainfall (WSHR) and 528 frontal heavy rainfall (FHR) events are identified by using the hourly precipitation data of 124 national rain gauge stations in South China from 1981 to 2020. The frequency of heavy rainfall events in South China presents an overall increasing trend, mainly due to the increase of WSHR events in Guangxi. The monthly frequency of FHR events in Guangxi is always higher than that in Guangdong from April to September, particularly in July, while WSHR events occur more (less) frequently in Guangdong than in Guangxi in April, May, and August (June and July). The FHR events mainly start around 0000 BST (Beijing Standard Time), while the start time of WSHR events is relatively evenly distributed from 2300 to 0300 BST. Synoptic circulations of WSHR events are objectively classified into five types, which reveals the difference of intensity and location of synoptic-scale systems (the western Pacific subtropical high, vortex, shear line, synoptic low-level jet, boundary layer jet) and precipitation among the five-type events. The occurrence frequency of Type 1 WSHR events in Guangxi peaks in June, while that of Type 2 varies greatly in Guangxi and Guangdong. The start time of Type 1 WSHR events has two peaks at 0100 BST and 0800 BST, while the start time of other four types is mainly within 2300 BST–0400 BST. The mean duration of each type WSHR events is about 10–25 h with shortest for Type 4 WSHR events and longest for Type 5.

1 Introduction

Heavy rainfall is the primary weather-related disaster in South China (Xia et al. 2006; Sun et al. 2019; Wu et al. 2020a, b). But its triggering mechanisms and predictability have always been a difficult problem for scientific research and operational weather forecast. Based on previous studies, heavy rainfall can be roughly classified into warm-sector heavy rainfall (WSHR) and frontal heavy rainfall (FHR) according to whether it is driven by weak or strong synoptic forcing (Huang et al. 1986; Ding 1994). The FHR is usually triggered by a front, which is often generated by the southward movement of cold air steered by the mid-latitude synoptic systems. Some of these frontal systems show the typical structure of a Meiyu front (Wu et al. 2020b). The WSHR often occurs in the warm sector, about 200–300 km away from the surface front or occurs in the convergence zone between the southwesterly and southeasterly airflows, or even in the southwesterly airflow without wind shear (Huang et al. 1986; Sun et al. 2019). Triggering mechanisms for WSHR are quite complicated, which may include topographic lifting, local thermal inhomogeneity, and land–sea breeze (Xia et al. 2006; Wang et al. 2011; Du and Chen 2018). The uncertainties in the triggering mechanisms make the forecasting of WSHR has long been a challenge in the operational weather forecast (Du and Chen 2018; Sun et al. 2019).

Responsible Editor: Clemens Simmer, Ph.D.

✉ Jianhua Sun
sjh@mail.iap.ac.cn

[1] Key Laboratory of Cloud-Precipitation Physics and Severe Storms, Institute of Atmospheric Physics, Chinese Academy of Sciences, Chaoyang District, P.O. Box 9804, Beijing 100029, China

[2] Collaborative Innovation Center on Forecast and Evaluation of Meteorological Disasters, Nanjing University of Information Science and Technology, Nanjing 210044, China

[3] University of Chinese Academy of Sciences, Beijing 100049, China

[4] International Center for Climate and Environment Sciences, Institute of Atmospheric Physics, Chinese Academy of Sciences, Beijing 100029, China

Published online: 26 December 2022

Previous studies have analyzed the statistical characteristics of heavy rainfall events in South China (Chen et al. 2012; Wang et al. 2014; Liu et al. 2019a; Wu et al. 2020a; Li and Du 2021). Chen et al. (2012) documented that the occurrence frequency of WSHR events is relatively low before the onset of the South China Sea (SCS) summer monsoon, but it increases significantly after the monsoon onset. Wang et al. (2014) used the daily precipitation data to analyze the statistical characteristics of persistent heavy rainfall events over South China and found that non-typhoon persistent heavy rainfall events in South China are concentrated in June and July, and that their frequency and intensity show an interdecadal increase. Liu et al. (2019a) found that WSHR events in South China mainly occur from April to July, with the maximum frequency in June and an average duration of 11.58 h. By using 12 years of hourly rain gauge data, Wu et al. (2020a) identified the WSHR events and FHR events in Guangdong and found that the frequency of WSHR events increases markedly from April to June, which is closely related to the onset of summer monsoon, whereas the FHR events show an unobvious monthly variation. By analyzing the relationship between heavy rainfall events and low-level jets (LLJ), Li and Du (2021) demonstrated that most WSHR events occur in the coastal areas in the early morning, and they are mainly caused by the interaction between boundary layer jets and the land wind at night, whereas the FHR events are mainly concentrated in the inland.

Due to the complex formation mechanisms, most WSHR events cannot be predicted accurately by numerical models. Therefore, researchers and forecasters often focused on the weather systems and environmental conditions related to WSHR (Sun et al. 2019). Huang et al. (1986) first classified the synoptic weather pattern of heavy rainfall in South China into four types: the warm shear line, the LLJ along coastlines, the prefrontal LLJ, and cold fronts or quasi-stationary fronts. Lin (2006) divided the synoptic background of the WSHR events into three categories: the backflow WSHR that is caused by the converging flows or warm-wet wind shear behind a transformed cold high pressure, the WSHR caused by a strong southwestern monsoon surge or southwestern LLJ, and the WSHR produced by the upper-level trough and subtropical LLJ. Chen et al. (2012) categorized WSHR events into three types according to the main influencing weather systems: the shear-line type, the low vortex type, and the southerly wind type. He et al. (2016) divided synoptic circulations of WSHR into three patterns: boundary layer convergence, southerly convergence, and strong southwest jet. Liu et al. (2019a) categorized the synoptic circulations of WSHR into four patterns: wind shear, low vortex, southern wind, and backflow. Classifications in these studies were all processed subjectively.

However, the application of objective classification method in meteorology can be traced back to the 1960s (Richman 1981). The commonly used objective classification methods can be roughly divided into four categories, i.e., the methods based on eigenvectors (Richman 1981; Huth 1996), such as the T-mode principal component analysis (PCT) which has been widely used in circulation classification in recent years (Xu et al. 2016; Miao et al. 2017; Liu et al. 2019b; Dong et al. 2020; Ning et al. 2020; Yang et al. 2021a, 2021b), the methods based on the leader algorithm, such as the Kirchhofer method (KIR; Blair 1998; Han et al. 2018), the hierarchical cluster analysis (HCL), and the methods based on the optimization algorithms (Hoffmann and Schlünzen 2013), such as the k-means algorithm (KMN) and k-medoids algorithm (KMD). Generally, geopotential height fields or sea-level pressure fields are commonly used as the meteorological variables for circulation classification in previous studies (Hoffmann and Schlünzen 2013; Xu et al. 2016; Tang et al. 2021; Yang et al. 2021a; Huang et al 2022; Liu et al. 2022).

Additionally, determination of classification number is essential for objective classification, but there is no unified or effective way to determine the number (Huth et al. 2008). For a good classification result, both the homogeneity within classes and the differences between classes need to be large enough. However, with the increase of classification number, the former will increase, and the latter will decrease, which leads to a dilemma on the classification number. Ways to determinate classification number vary from study to study without a universal approach or methodology (Hoffmann and Schlünzen 2013; Miao et al. 2017; Tang et al. 2021; Yang et al. 2021b). However, previous studies have classified the synoptic circulations of WSHR events over South China into 3–5 patterns (Lin 2006; Chen et al. 2012; He et al. 2016; Liu et al. 2019a, 2021), which provided a physical basis for the current study.

In the current study heavy rainfall events in South China are identified and categorized into WSHR and FHR by using the hourly precipitation data from China Meteorological Administration (CMA) and the fifth-generation ECMWF (European Centre for Medium Range Forecasts) reanalysis (ERA5) data. Then, the statistical characteristics of the two different types of heavy rainfall events are compared and analyzed. Furthermore, the synoptic circulations of WSHR in South China are objectively classified into different patterns by using the *k*-medoids algorithm. The remainder of this paper is organized as follows: Section 2 presents the introduction of the data and methodology. Statistical characteristics of WSHR and FHR events in South China are compared in Sect. 3. Section 4 presents classification of synoptic circulations for WSHR and their statistical characteristics. Finally, a summary is given in Sect. 5.

2 Data and methodology

2.1 Data

The hourly precipitation data from 2420 national rain gauge stations from 1981 to 2020 provided by CMA is used in this study for identifying the heavy rainfall events. The rotated empirical orthogonal function (REOF) analysis was applied to detect the spatial modes of hourly precipitation of eastern China (Li et al. 2016). Adjacent stations with accumulated variance contribution ≥ 60% were considered to have the same spatial pattern and should be categorized into one climatic region. The same method was used to select 124 stations to represent South China (Liu et al. 2019a). In the current study, the same 124 stations are chosen to represent South China (~ 105°–117° E, 21°–26° N), including 42 in Guangdong, 70 in Guangxi, 8 in Hunan, 3 in Jiangxi, and 1 in Yunnan (Fig. 1a).

The ERA5 dataset (Hersbach et al. 2020) with a spatial resolution of 0.25° × 0.25° and temporal resolution of 1 h from April to September in 1981–2020 is used to determine the position of front on vertical cross sections and to analyze the circulation patterns. In addition, the tropical cyclone (TC) best-track dataset provided by the CMA (Ying, et al. 2014; Lu, et al. 2021) is used to exclude the heavy rainfall events influenced by TCs.

2.2 Identification and categorization of heavy rainfall events

A heavy rainfall event is defined following Liu et al. (2019a) according to two criteria: at least three adjacent (with distances between each other ≤ 150 km) stations record daily precipitation ≥ 50 mm; each of above stations records at least one continuous 3-h period during which hourly precipitation ≥ 5 mm and accumulative 3-h precipitation ≥ 30 mm. Here daily precipitation refers to total precipitation during 0000–2400 UTC. The station satisfying those criteria and recording the maximum daily precipitation is defined as representative station. In range of 150 km from the representative station, the time at which hourly precipitation ≥ 5 mm first (last) recorded is defined as the start (end) time of heavy rainfall event. Heavy rainfall events due to TCs are excluded according to distances between the representative station and the TC center. If the distance between the representative station and the TC center is less than given distance threshold according to the intensity of TC (Table 1), the heavy rainfall event is considered to be related to TC and is excluded.

Generally, WSHR events are not affected by synoptic fronts and often occur under weak synoptic-scale forcing, while FHR events are closely related to synoptic fronts. To distinguish WSHR and FHR, existence and location of the front are determined by examining the vertical meridional cross section of pseudo-equivalent potential temperature field along the representative station at the start time of the heavy rainfall event. If a front exists and the representative station is located within 200 km from it, the heavy rainfall event is classified into FHR events. Otherwise, the heavy rainfall event is classified into WSHR events.

2.3 Classification of synoptic circulation pattern

According to the distribution of the above 124 national stations and considering that WSHR events in South China mostly occur under the influence of southerly flow, the synoptic circulation classification domain for WSHR events is defined as 100°–125°E, 10°–30°N (the pink box in Fig. 1a).

Four objective classification methods (i.e., PCT, KIR, HCL, and KMD) are employed to classify the synoptic circulation for WSHR events. Firstly, we investigate their performance at different classification numbers (i.e., 4, 8, 12, 16) by evaluating six different evaluation indices (i.e., the explained cluster variance, the pseudo-F statistic, the within-type standard deviation, the confidence interval of the mean, the confidence interval of the mean, the silhouette index). Base on the results, the KMD method has been chosen to classify circulations of WSHR events in South China. In order to obtain a meaningful result, we have considered both the results of objective evaluations and the actual circulation types in previous studies and decided that the number 5 is the optimal choice which has been used in the current study. Detailed procedures of determining classification method and number are in the supplementary information.

South China is in the transition zone between tropics and subtropics where the geopotential height gradient is quite weak. Therefore, only using the geopotential height for classification cannot achieve efficient results. In addition, the synoptic systems associated with WSHR events are more likely to be the convergence or shear lines of the wind field rather than the systems in the geopotential height field (e.g., trough and low pressure; Liang et al. 2019; Wu et al. 2020b; Chen et al. 2021; Li and Du 2021; Liang and Gao 2021). As the moisture transport is very important to heavy rainfall events (Wang et al. 2016; Sun et al. 2018; Zhang et al. 2021b) and the weather systems related to WSHR events in South China are mostly important in the lower troposphere (Wu et al. 2020b; Yin et al. 2020; Liang and Gao 2021), the geopotential height, wind field, and moisture flux at 850 hPa and 925 hPa are used in the classification of WSHR events in South China.

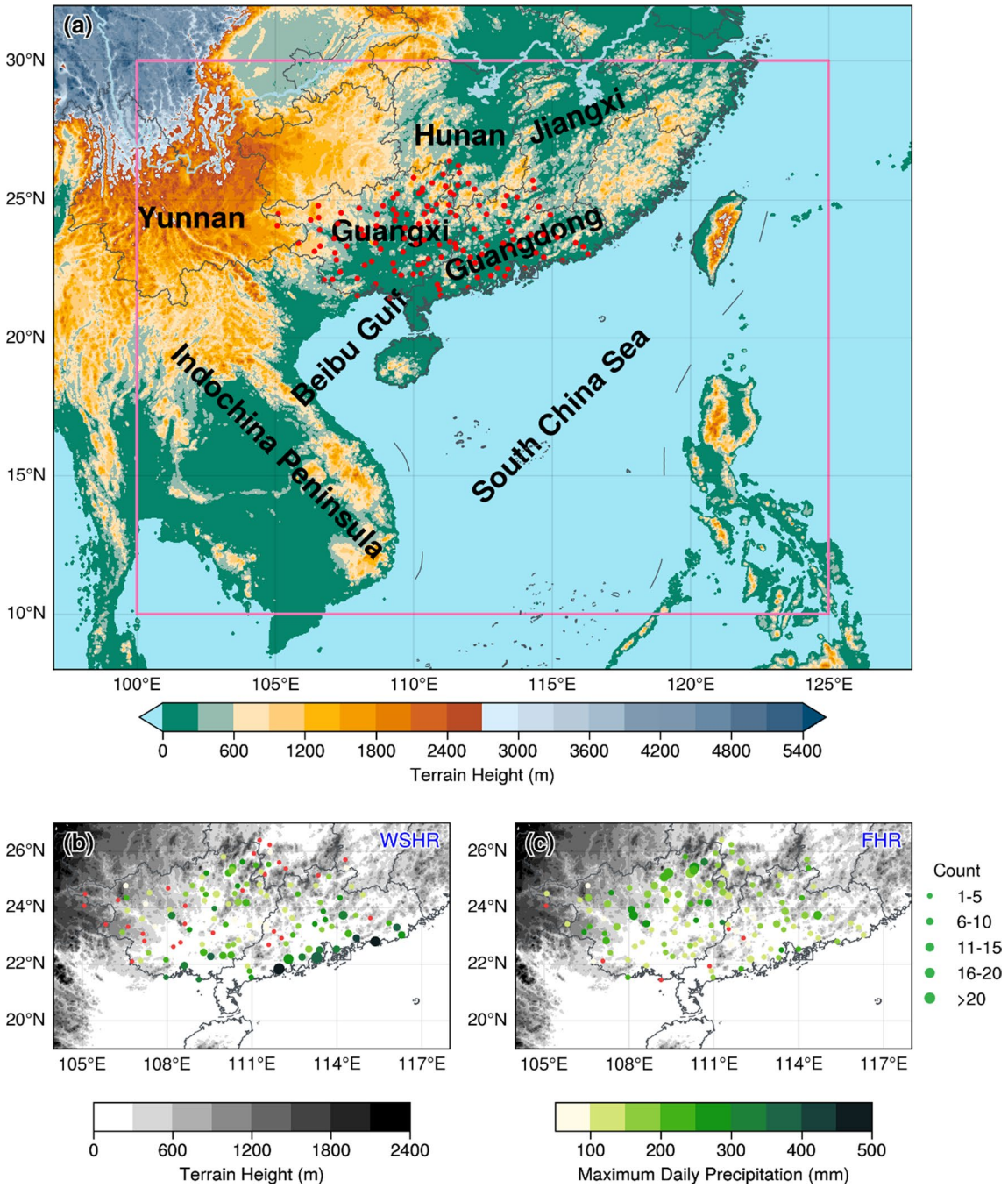

Fig. 1 **a** Distribution of national meteorological stations in South China (red dots) and terrain height (shading; m). The pink box represents the domain for synoptic circulation pattern classification. **b** Spatial distribution of WSHR events. The sizes and colors of dots represent the occurrence numbers and the maximum daily precipitation of WSHR events, respectively. Gray shading denotes terrain height. The red dots indicate that the stations have never been identified as representative stations. **c** As in (**b**) but for FHR events

3 Statistical characteristics of WSHR and FHR events

According to the criteria in Sect. 2b, 930 heavy rainfall events are identified in South China from 1981 to 2020. The WSHR events mostly occur in the coastal areas (the south of Guangdong and the southeast of Guangxi) and the windward slopes of mountains (the middle of Guangdong and the northeast of Guangxi) (Fig. 1b). The FHR events mostly occur in the mountainous areas of northern Guangxi (Fig. 1c). This distribution is consistent with previous studies (Wu et al. 2020a; Li and Du 2021; Du et al. 2022). A

Table 1 Distance thresholds of TC influence

Grade of tropical cyclones	Distance threshold (km)
Tropical depression	200
Tropical storm	300
Severe tropical storm	400
Typhoon and above	500

Table 2 Number and corresponding proportion of the five different types of WSHR events

	Number	Proportion (%)
Type 1	110	27.3
Type 2	106	26.3
Type 3	67	16.7
Type 4	55	13.7
Type 5	64	15.9
Total	402	100

total of 27 (6) stations have never been identified as representative stations in WSHR (FHR) events from 1981 to 2020, and the maximum daily precipitation in WSHR (FHR) events is 493.7 mm (329.4 mm). These features indicate that WSHR events tend to occur over several specific areas in South China, yet FHR events are more evenly distributed.

The most frequent year is 2008 with a total amount of 41 heavy rainfall events, and the least frequent year is 1991 with a total amount of 9 (Fig. 2a). The total amount of WSHR events is 402 (Table 2), and the highest frequent year is 2008 with a total amount of 20. The total amount of FHR events is 528, and the highest frequent year is 2010 with a total amount of 25. As shown in Fig. 2a, both WSHR and FHR events show an increasing trend, with the growth rate of 1 per decade and 0.1 per decade, respectively. To investigate the regional characteristics of the frequency of heavy rainfall events in South China, the frequencies of WSHR and FHR (Fig. 2c) events in Guangdong and Guangxi are further analyzed (Fig. 2b). The frequency of WSHR events in Guangdong increases slightly with a change rate of 0.16 per decade, while that in Guangxi increases significantly with a change rate of 0.82 per decade. As for FHR events, the frequency increases slightly in Guangdong and decreases

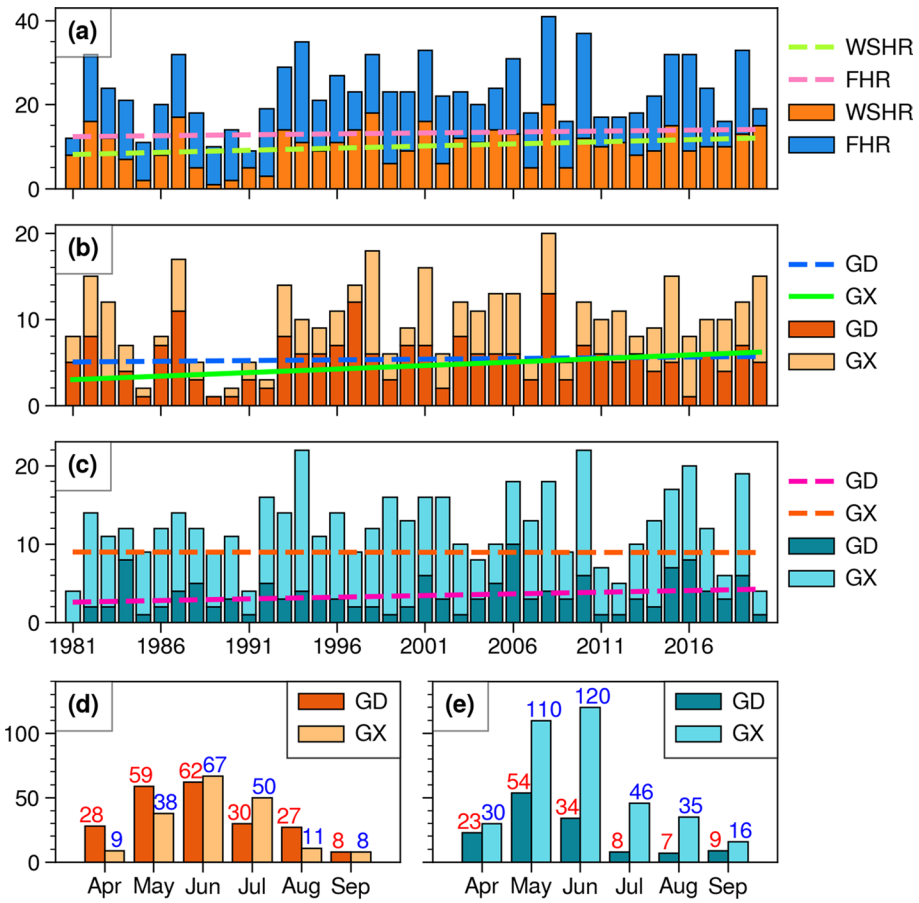

Fig. 2 **a** Interannual variation of heavy rainfall event frequency in South China with orange and blue bars representing WSHR and FHR, respectively; **b** interannual variation of WSHR frequency in South China with dark and light orange bars representing WSHR in Guangdong and Guangxi, respectively. **c** The same as (**b**) but for the FHR. **d** Monthly variation of WSHR frequency. **e** The same as (**d**) but for the FHR. The lines represent occurrence frequency trends, in which the solid one indicates that the change rate exceeds the 95% statistical significance according to a *F* test. The occurrence frequencies of WSHR and FHR events in Guangdong (Guangxi) of each month are labeled above the bars in red (blue) in (**d**) and (**e**)

slightly in Guanxi. It is clearly shown that the increase of heavy rainfall events in South China is mainly caused by the increase of WSHR events in Guangxi.

Figure 2d, e exhibits the monthly variations of WSHR and FHR events in South China. The frequencies of WSHR events in Guangdong and Guangxi both peak in June (62 and 67, respectively), but there are some differences in other months. WSHR events occur more (less) frequently in Guangdong than in Guangxi in April, May, and August (June and July), indicating a conversion of WSHR frequency between Guangdong and Guanxi in late May or early June. This may be related to the seasonal adjustment of atmospheric circulations, that is, the onset of SCS monsoon in late May (Kajikawa and Wang 2012; Huangfu et al. 2017; Luo and Lin 2017). However, FHR events show different monthly variations from WSHR events. Their frequency in Guanxi peaks in June (120), while that in Guangdong peaks in May (54), and the former is always higher than the latter from April to September, particularly in July (46 versus 8).

Figure 3 shows the frequency diurnal variations of the start time and end time of WSHR and FHR events. The start time of WSHR and FHR events in South China is generally at night, but there are some differences. The start time of FHR events is mainly concentrated at 2200–0300 Beijing Standard Time (BST, BST = UTC + 8 h), with the peak at 0000 BST, while the start time of WSHR events is evenly distributed from 2300 to 0300 BST. Since WSHR events mostly occur in the coastal areas or the windward slope of mountains (Fig. 1b), their triggering at night may be related to the intensification of low-level convergence caused by the interaction between the onshore monsoon flows and the downslope winds/land breezes (Bai et al. 2019). The triggering for FHR events at night may attribute to two mechanisms: the intensifications of LLJs at night and the subsequent enhancements of moisture transport, low-level convergence, and convective instability (Guan et al. 2020; Zeng et al. 2019, 2022; Huang et al. 2022), and frontogenesis caused by the diabatic process, i.e., the combination of sensible cooling, condensational heating, and evaporative cooling (Bannon and Mak 1984; Chen et al. 2007; Wang et al. 2022). The nocturnal LLJs enhance the horizontal convergence or mesoscale ascent at night due to the southerly which helps trigger FHR events over front area at their northern terminus (Zeng et al. 2022). During frontal precipitation, the frontogenesis is dominated by diabatic heating (Wang et al. 2022). At the warm side of the front, the combination of condensational heating and evaporative cooling is negligible at the early stage since the precipitation is relatively small (Cartwright and Ray 1999; Reeves and Lackmann 2004). However, at the cold side of the front, sensible cooling over cloud-free areas increases the temperature gradient, causes frontogenesis (Chen et al. 2007), and subsequently triggers the FHR events during night.

The end time of WSHR and FHR events is both concentrated in the daytime (Fig. 3b). FHR events are likely to end in the morning and noon, probably due to the weakening of temperature gradient on the two sides of the front during daytime (Chen et al. 2007). WSHR events prefer to end in the afternoon. Previous studies have shown that the maintenances of WSHR events are closely related to the LLJs, including the interaction between LLJs and topography (Du and Chen 2019) and the convergence of LLJs and the local land/mountain breezes (Wu et al. 2020a; Li and Du 2021). Since the occurrences of LLJs are minimum (Du et al. 2014) and the intensities are weakest (Du and Chen 2019) in the afternoon, it can be inferred that the end of WSHR events in the afternoon is mainly related to the weakening of LLJs.

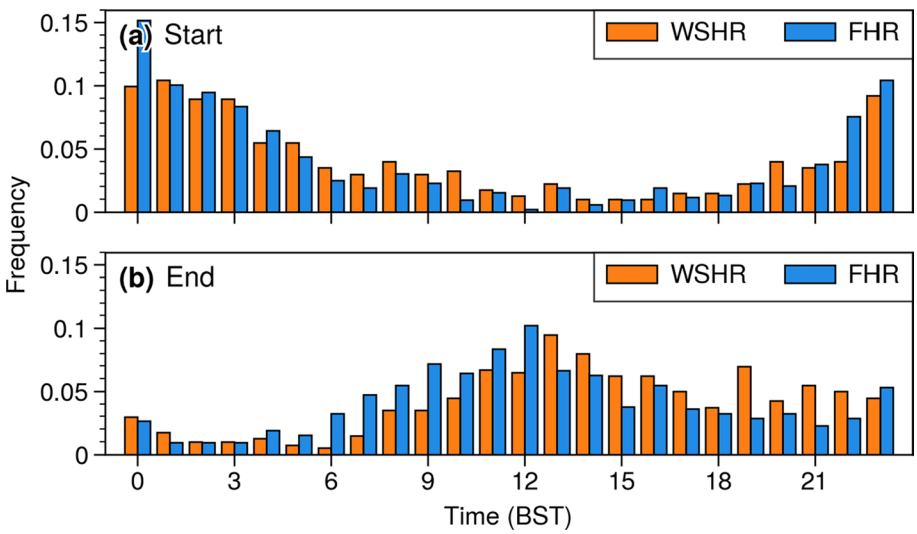

Fig. 3 Frequency diurnal variations of start time and end time of (**a**) WSHR and (**b**) FHR events. Orange and blue bars represent WSHR and FHR, respectively

4 Classification of WSHR events in South China

4.1 The classified synoptic circulation patterns

WSHR events are classified by the KMD method introduced in Sect. 2c. The number and corresponding proportion of the five different types of WSHR events are shown in Table 2. The synoptic circulations corresponding to the start time of WSHR events in each type are synthetically analyzed and the composite fields of each synoptic circulation pattern are shown in Figs. 4, 5, 6, 7, 8. The objective classification results represent not only the major characteristics of circulation but also the distribution of rain belts or rainfall centers. To verify the representativeness of the composite fields of each synoptic circulation pattern, five typical WSHR events of each type are selected for further analysis. There are 110 WSHR events of Type 1, accounting for 27.3% (Table 2). For Type 1 (Fig. 4a), the western Pacific subtropical high (WPSH), which is indicated by the 5880-gpm contour at 500 hPa, is located to the east of the SCS, and South China is mainly influenced by the southwesterly airflow. The southwesterly airflow is formed by the confluence of two flows, one of which extends from Indochina Peninsula to the mainland of South China through Beibu Gulf and the other extends from the SCS to the mainland, converging with the first one in the coastal area of South China. Zhang and Meng (2019) indicated that the mean height of synoptic low-level jets (SLLJ) and boundary layer jet (BLJ) are ~ 800 hPa and ~ 930 hPa in South China, respectively. Therefore, the SLLJ (BLJ) is defined as the wind with speed exceeding 8 m/s at 850 hPa (925 hPa) in the present study. The positions of SLLJ and BLJ are close on the whole, but there are some differences in the location of jet cores (Fig. 4a). The BLJ core is to the south of the SLLJ core and is located in the coastal area, while the SLLJ core is located inland. Hourly mean precipitation is widely distributed in the north of Guangxi (Fig. 4c). The typical WSHR event for Type 1 started at 0700 BST on June 27, 1988 and lasted for 31 h. The precipitation was widely distributed in the north of Guangxi, with the maximum hourly value of 67.6 mm and the maximum total amount of 276.5 mm (Fig. 4d). The location and intensity of SLLJ in the event were basically the same as those in the composite analysis, but the BLJ was located more northerly in the event (Fig. 4b). There was a TC to the south of WPSH in the event and the southwesterly over Indian Ocean was stronger than that in the composite field, which may provide moisture for the WSHR event. The

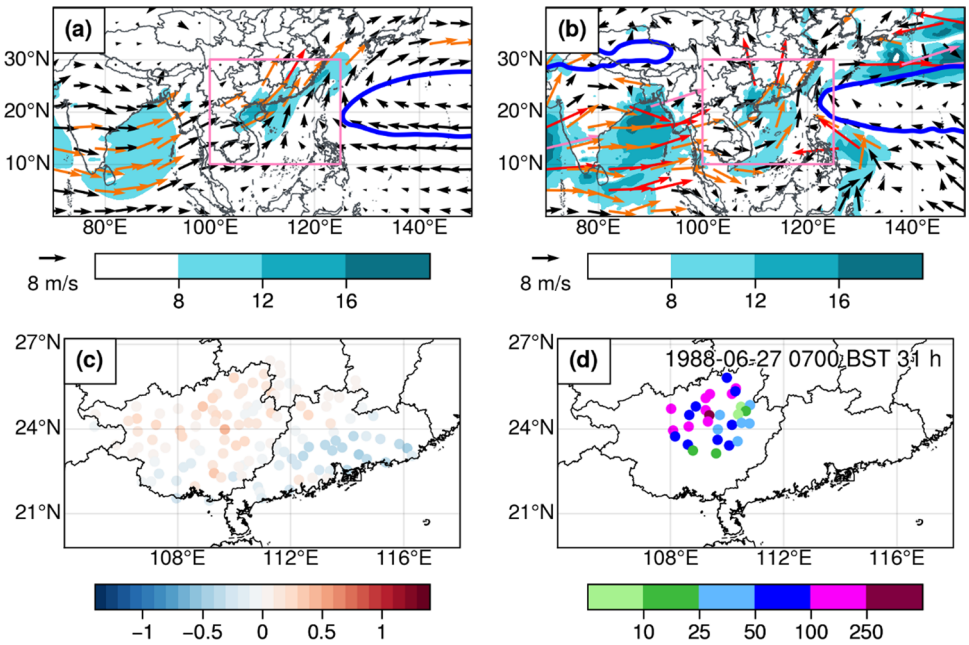

Fig. 4 Synoptic circulations of **a** composite field and **b** typical event for the Type 1 warm-sector heavy rainfall (WSHR) in South China. The pink box indicates the classification domain. Blue contours refer to the 5880 gpm at 500 hPa. Vectors refer to wind at 850 hPa, of which orange (red) ones indicate that wind speed exceeds 8 (12) m/s. Shaded areas indicate that wind speed exceeds 8 m/s at 925 hPa. **c** Hourly mean precipitation deviation (mm) of Type 1. Hourly mean precipitation is calculated based on the events at every station within a radius of 150 km around representative stations, and the deviations are obtained by subtracting hourly mean precipitation of all WSHR events from hourly mean precipitation of events in each type. **d** Cumulative precipitation (mm) of typical event for Type 1. The time corresponding to (**b**) is the start time of the event, which is labeled on (**d**) together with the duration of the event

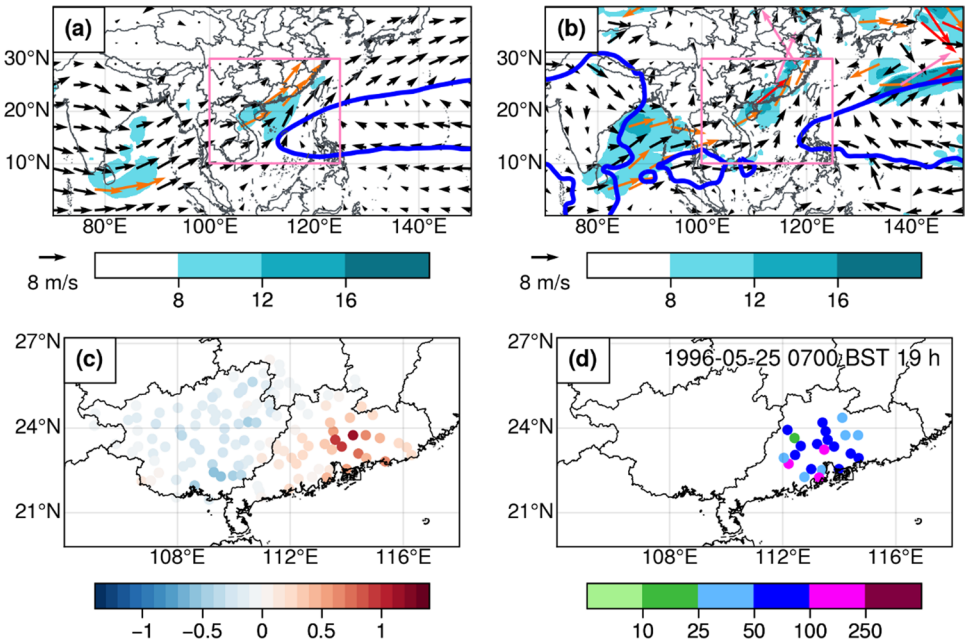

Fig. 5 The same as Fig. 4, but for Type 2

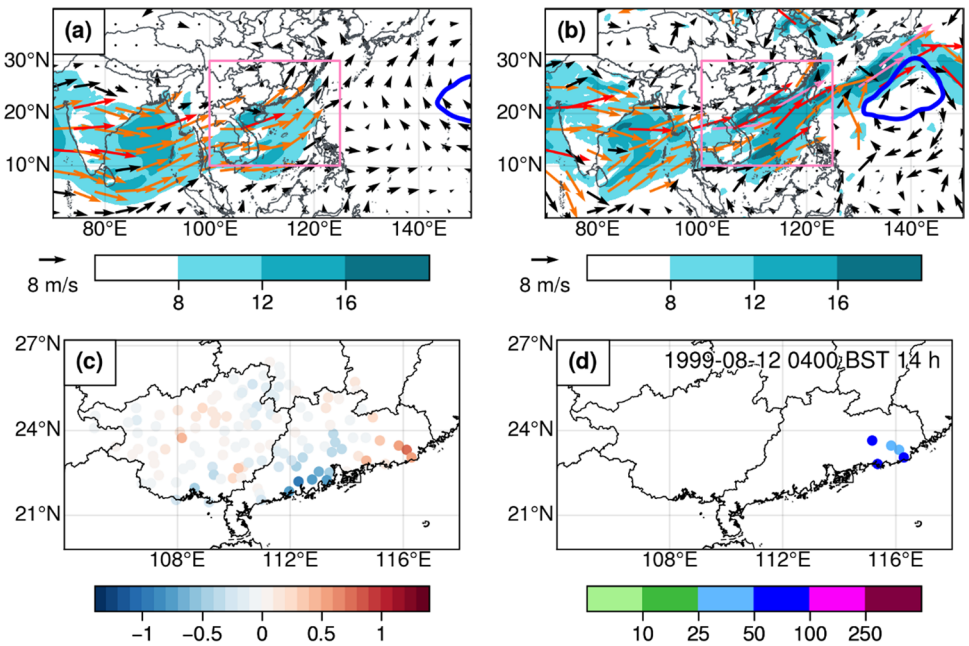

Fig. 6 The same as Fig. 4, but for Type 3

precipitation was distributed in the mountainous areas of northern Guangxi. The convergence caused by the interaction between SLLJ and terrain acted as a triggering mechanism for the event.

There are 106 events of Type 2 accounting for 26.3%. The WPSH extends westward to the middle of the SCS, and most of South China is influenced by the southwesterly airflow except for the northern Guangxi (Fig. 5a), which is under the influence of a shear line. Compared with the circulation in Type 1 (Fig. 4a), the southwesterly airflow in Type 2 is slightly weaker, which is probably due to the location and shape of the WPSH. Both SLLJ and BLJ are weaker without obvious jet cores than those in Type 1. The high-value centers of hourly mean precipitation corresponding to Type 2 are relatively concentrated in the middle of Guangdong (Fig. 5c). It can be seen that precipitation center is located between the shear line and BLJ (close to BLJ), so the heavy precipitation is caused by both the shear line and the jet. The selected WSHR event of Type 2 started at 0700 BST on May 25, 1996 and lasted for 19 h. The precipitation was widely distributed from southern to central Guangdong, with the maximum hourly rainfall of 69.4 mm and the maximum

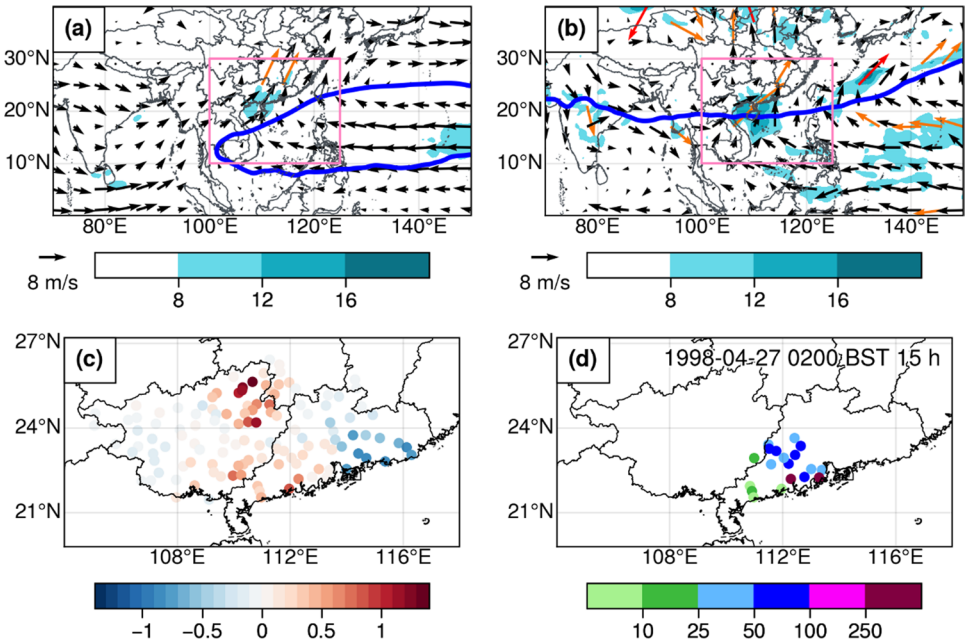

Fig. 7 The same as Fig. 4, but for Type 4

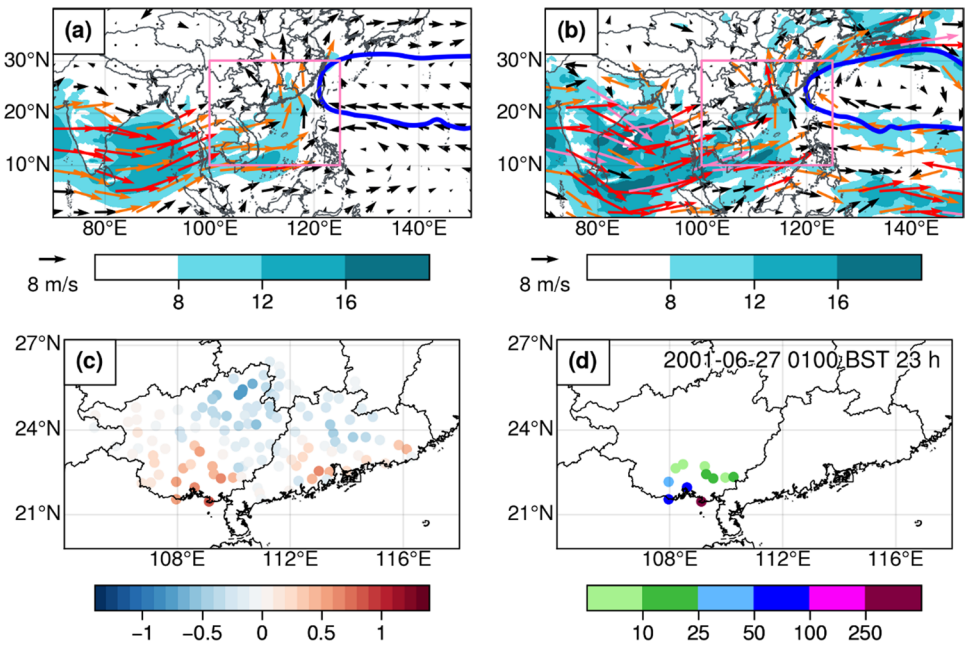

Fig. 8 The same as Fig. 4, but for Type 5

cumulative rainfall of 148 mm (Fig. 5d). The WPSH was a little easterly than that in the composite analysis (Fig. 5b). The intensity (location) of SLLJ in the event was stronger than (roughly the same as) that in the composite field. As for BLJ, the location was more northerly, and the intensity was stronger than that in the composite field.

The total proportion of the first two types of WSHR events reaches 53.6%, and the proportions of the other three types are 16.7%, 13.7%, and 15.9%. Type 3 (67 events) is characterized by the strong low-level southwesterly airflow (Fig. 6a), due to the eastward retreat of WPSH to the central Pacific. A weak vortex is located in northern Guangxi. Its vertical extension is quite shallow, obvious only at 700 hPa, and it gradually turns to be a shear line below 700 hPa. The WSHR events are usually far from the shear lines and often occur at the coastal areas or on the southern slope of mountains. It is indicated that the shear lines are more likely to regulate the large-scale circulation than directly cause the WSHR events. SLLJ and BLJ in Type 3 are considerably strong, extending from the Bay of Bengal to the mainland of South China through the Indochina Peninsula. The BLJ core is located

in Beibu Gulf and the SLLJ core is slightly southerly. The corresponding high-value centers of hourly mean precipitation are located in northwestern Guangxi, southeastern Guangxi, and southeastern Guangdong (Fig. 6c), which may be caused by different mesoscale convective systems under the influences of the vortex/shear line, the BLJ, and SLLJ. The typical WSHR event of Type 3 began at 0400 BST on August 12, 1999 and lasted for 14 h. The precipitation was concentrated in a small region in southeastern Guangdong, with a maximum hourly record of 28.8 mm and a maximum total precipitation of 79.1 mm (Fig. 6d). Although both SLLJ and BLJ were quite strong in this event (Fig. 6b), the moisture passed through South China instead of staying there, resulting in weak moisture convergence, less precipitation, and short duration of this event.

Type 4 has only 55 events, which is the least of all five types of WSHR events. The synoptic circulation of Type 4 (Fig. 7a) shows that South China is on the north side of the WPSH that controls the SCS and is under the influence of the southerly airflow which consists of two branches. One is the southwesterly airflow from the Indochina Peninsula and the other is the southeasterly airflow from the western Pacific through the SCS. The eastern Guangdong is influenced by the southeasterly airflow, and the other areas are influenced by the southwesterly airflow. The SLLJ and BLJ of this type are weakest among the five types. Four backflow WSHR events studied by some researchers before are all classified into Type 4 (Ye and Miao 2014; Ye and Xu 2014; Lin et al. 2015, 2020), suggesting that this type reflects the major characteristics of backflow WSHR events to some extent. There are two high-value centers of hourly mean precipitation in Type 4 (Fig. 7c), with one located at the junction of southwestern Guangdong and southeastern Guangxi and the other located in the northeastern Guangxi. The formation of first precipitation center may be related to the convergence of the southwesterly and southeasterly flows, and the second and the third are related to the low-level jet and terrain. The selected WSHR event of Type 4 started at 0200 BST on April 27, 1998 and lasted for 15 h. The precipitation of the event was widely distributed in southwestern Guangdong, with the maximum hourly precipitation of 102 mm and the maximum cumulative precipitation of 281.2 mm (Fig. 7d). The controlling area of WPSH in the event was wider than that in the composite field, but the low-level circulation was basically the same from Indian Ocean to SCS (Figs. 7a, b). The SLLJ in this event had the similar intensity as that in the composite field but the location was slightly southerly. As for BLJ, the intensity in this event was stronger and the controlling area was larger. The entrance of BLJ in this event had extended southward to the middle of the SCS, which was more conducive to the moisture transportation to the rainfall area.

As for Type 5 (Fig. 8a), the WPSH is to the northeast of South China. A strong vortex controls the southeastern Guangxi, while other areas in South China are influenced by the southeasterly airflow which splits into two branches in the north of South China. Hourly mean precipitation centers in Type 5 are in southern Guangxi and the coastal areas of Guangdong (Fig. 8c). The former center may be related to the vortex and land–sea breeze (Wen et al. 2010), the latter center may be caused by the interaction between BLJ and coastal terrain. The typical WSHR event of Type 5 began at 0100 BST on June 27, 2001 and lasted for 23 h. The circulation of this event was consistent with that of composite field, characterized by the same positions of WPSH and the vortex, and the similar locations and intensity of SLLJ and BLJ (Fig. 8b). The precipitation of this event was distributed near the coast of Guangxi, with the hourly maximum of 107.9 mm and the maximum cumulative precipitation of 341.8 mm (Fig. 8d).

In Type 4 (Fig. 7a) and Type 5 (Fig. 8a), Guangdong is under the influence of the southeasterly airflow, but there are some differences. The easterly airflow in Type 5 is to the south of WPSH and the associated anti-cyclonic circulation is also consistent with WPSH, which indicates that the southeasterly airflow in this type is generated by the WPSH. However, the southeasterly airflow in Type 4 does not coincide with the 5880-gpm contour of WPSH. As WSHR events in this type mainly occur in April and May, the southeasterly airflow in Type 4 may be related to the transformed surface cold high on the sea, which is also consistent with the characteristics of backflow WSHR events.

4.2 Statistical characteristics

Monthly variations of WSHR occurrence frequency for each type are shown in Fig. 9. For Type 1 (Fig. 9a), WSHR events mainly occur from April to June in Guangdong and from May to July in Guanxi. As for Type 2 (Fig. 9b), WSHR events in Guangdong mainly occur from April to June, which is similar with Type 1 but with the highest frequency in May rather than in June as in Type 1. WSHR events in Guangxi occur much less frequently than those in Guangdong, mainly in April, May, and June. WSHR events of Type 3 (Fig. 9c) mostly occur from June to August, and those of Type 4 (Fig. 9d) mainly in April and May. As for Type 5 (Fig. 9e), WSHR events relatively evenly occur in June, July, and August. It is clear that the monthly variation of different type WSHR is associated with the variation of synoptic circulation.

To investigate the similarities and differences of diurnal variation characteristics of the five types, the frequencies of start time and end time, precipitation perturbation and duration distribution of each type are shown in Fig. 10. In general, start time of these five types is mostly at night,

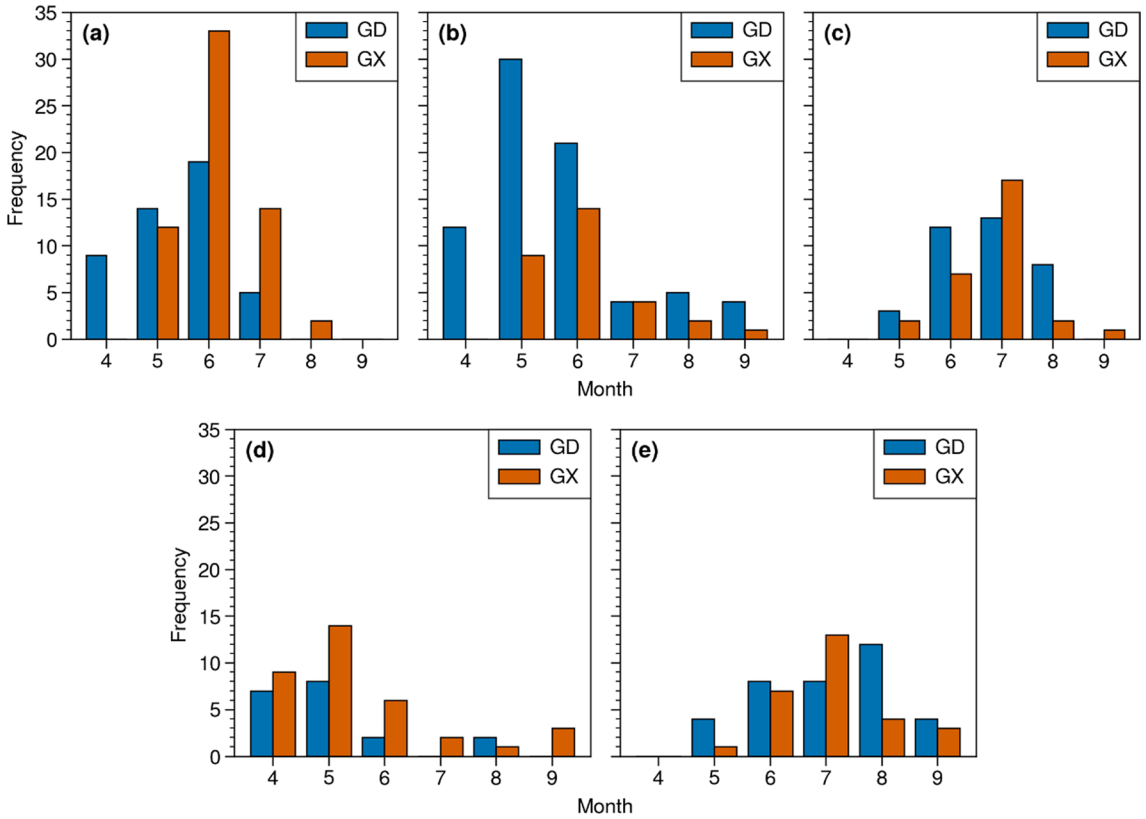

Fig. 9 Monthly variations of WSHR frequency for each type. **a** Type 1, **b** Type 2, **c** Type 3, **d** Type 4, and **e** Type 5. GD and GX denote Guangdong and Guangxi, respectively

which is consistent with the diurnal variation for all WSHR events (Fig. 3a). There are two peaks of start time for Type 1 (Fig. 10a), namely 0100 BST and 0800 BST. Start time of Type 2 (Fig. 10e) is concentrated within 0100–0300 BST, of which 0100 BST counts the most. The frequency of start time reaches the highest at 2300 BST for Type 3 (Fig. 10i). The frequency of start time for Type 4 (Fig. 10m) is concentrated within 0200–0400 BST and reaches highest at 0400 BST. As for Type 5 (Fig. 10q), the frequency of start time reaches highest at 0000 BST. In general, start time of WSHR events is mainly within 2300–0400 BST, which is mainly caused by the convection triggered at night.

In terms of end time, most WSHR events tend to end at noon or afternoon. For Type 1 (Fig. 10b), the events mainly end within 1300–1700 BST, with the least frequency at 1600 BST. As for Type 2 (Fig. 10f), the frequency of end time reaches highest at 2100 BST. The frequency of end time reaches highest at 1300 BST for both Type 3 and Type 4 (Figs. 10j, n, respectively). For Type 5 (Fig. 10r), the frequency of end time is relatively evenly distributed from 1100 to 1500 BST.

Hourly mean precipitation of a certain type is obtained by averaging precipitation of all stations within a radius of 150 km around the representative station at each hour of the whole duration. To further illustrate the diurnal variation of precipitation for each type, precipitation perturbations are calculated by subtracting the hourly mean precipitation of each type (Fig. 10c, g, k, o, s). Overall, precipitation mainly concentrates in early morning and late afternoon, consistent with the results found by Luo et al. (2016) that occurrence frequency of extreme hourly precipitation for weak-synoptic type over South China peaks at early morning and late afternoon.

The diurnal variations of precipitation for Type 1 (Fig. 10c), Type 3 (Fig. 10k), and Type 5 (Fig. 10s) show similar patterns, that is, precipitation mainly occurs at early morning, with the maximum at 0600, 0600, and 0200 BST, respectively. Precipitation of Type 1 mainly occur at the north of Guangxi (Fig. 4c), which is the high-value center of occurrence frequency for both extreme hourly precipitation and persistent heavy rainfall events (Chen 2018; Zhang et al. 2021a), showing early morning peaks similar as hourly precipitation of Type 1. Li and Du (2021) found that precipitation of WSHR events mainly occurs at three coastal areas, two of which are consistent with precipitation centers in Type 5 and Type 3, namely, the south of Guangxi and the southeast of Guangdong, and both show similar precipitation peaks at the early morning. Wu et al. (2020a) also identified

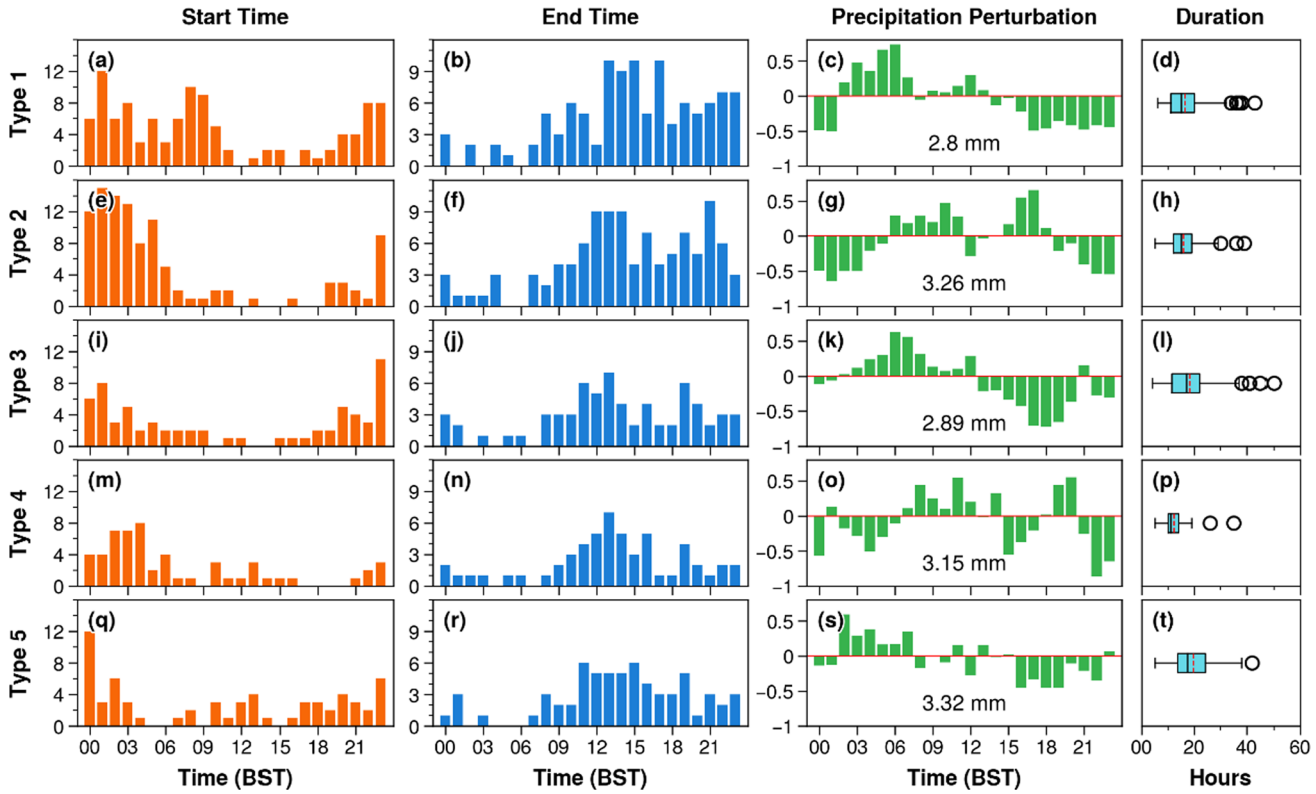

Fig. 10 Diurnal variations of start time (first column, unit: frequency), end time (second column, unit: frequency), perturbation of hourly mean precipitation (third column, unit: mm) of WSHR events for five types of WSHR events. The precipitation perturbation is obtained by subtracting mean value from hourly precipitation of each type. Box plots in the last column indicate the distributions of WSHR durations. The left and right edges of the box represent 1st quartile and 3rd quartile, respectively. Black solid lines and red dashed lines inside the boxes represent median and average value, respectively

the WSHR precipitation center on southeastern Guangdong with an early morning peak similar as in Type 3.

Precipitation of Type 2 (Fig. 10g) mainly occurs at morning and afternoon, with the peak at 1700 BST. WSHR events of Type 2 mainly occur in May and June (Fig. 8b), with the precipitation center located at central Guangdong (Fig. 5c). The diurnal variation of precipitation of Type 2 may be related to LLJ or local circulation, which should be further studied in future. The diurnal cycle of Type 4 (Fig. 10o) shows a different pattern with fluctuant diurnal phase and an after-sunset peak at 2000 BST, which may be caused by the combination of the shortest durations (Fig. 10p) and multiple precipitation centers (Fig. 7c).

The duration of Type 1 WSHR events (Fig. 10d) is roughly 11–20 h (first quartile to third quartile, the same below) with a median of 15 h and an average of 16.49 h. The durations of Type 2 and Type 3 (Figs. 10h, l, respectively) are 12–19 h and 11.5–22 h, respectively, basically consistent with that of Type 1. The duration of Type 4 WSHR events (Fig. 10p) is 10–14 h, relatively shorter than that of other types, with a median of 11 h and an average of 12.31 h. As for Type 5 (Fig. 10t), the duration is 13.75–24.25 h, with a median of 17.5 h and an average of 19.63 h, which is longest among five types, and this phenomenon may be related to the intensity of strong vortex and LLJ.

5 Summary and conclusion

Based on the hourly precipitation of 124 rain gauge stations in South China from 1981 to 2020 and the ERA5 reanalysis data, the heavy rainfall events in South China were identified and divided into WSHR and FHR, and the circulations associated with the WSHR were objectively classified by the KMD method. The main conclusions are as follows.

A total of 930 heavy rainfall events (402 WSHR events) were identified in South China from 1981 to 2020. The occurrence frequency of heavy rainfall events in South China shows an increasing trend from 1981 to 2020, mainly due to the increase of WSHR events, particularly in Guangxi. The monthly frequency of FHR events in Guangxi is always higher than that in Guangdong from April to September, especially in July. The occurrence frequency of WSHR events in Guangdong is much higher

than that in Guangxi in April, May, and August but lower in June and July. The start time of FHR events in South China is mainly around 0000 BST, while that of WSHR events is relatively evenly distributed from 2300 to 0300 BST. Both FHR and WSHR events end mainly in the daytime, but the former end mostly in the morning, while the latter mostly around noon.

The synoptic circulations of WSHR events in South China were objectively classified into five types by using the KMD method. The Type 1 WSHR events are mainly affected by the southwesterly airflow, and the precipitation areas are relatively scattered. The Type 2 WSHR events are affected by the interaction between the southwesterly airflow and the shear line, and the precipitation areas are mainly located in the middle of Guangdong. The SLLJ and BLJ in Type 3 are both the strongest. As for Type 4, WSHR events are mainly caused by the convergence of the southwesterly airflow and the southeasterly airflow, and the precipitation is correspondingly concentrated in the convergence zone of the two streams and the mountainous area to the north. The Type 5 WSHR events are mainly affected by the vortex and the southerly wind.

There are obvious differences in monthly, diurnal variations, and duration of the five different WSHR types. The monthly variation of two major types shows that the frequency of Type 1 WSHR events in Guangxi peaks in June, while that of Type 2 varies greatly in Guangxi and Guangdong. The frequency of start time for Type 1 has two peaks at 0100 BST and 0800 BST, while the start time of other types is mainly concentrated in 2300–0400 BST. Two end time peaks appear in Type 2, which are at 1200 BST–1400 BST and 2100 BST, and the end time of other types is mainly within 1100 BST–1700 BST. The main duration of all WSHR events is about 10–25 h. The duration of Type 4 WSHR events is shortest, while that of Type 5 is longest.

In summary, this study analyzed the spatio-temporal characteristics and the objective classifications of the WSHR events in South China (Guangdong and Guangxi). However, in-depth discussion on their formation mechanisms is not conducted. The relationships between these statistical characteristics and the corresponding synoptic circulations, mesoscale convection, and their formation mechanisms in different circulation patterns need to be investigated in future.

Supplementary Information The online version contains supplementary material available at https://doi.org/10.1007/s00703-022-00949-8.

Acknowledgements The authors are grateful to the National Meteorological Center, China Meteorological Administration for providing the precipitation observations used in the present study. This research was supported by the National Key Research and Development Program of China (No. 2019YFC1510400), the Strategic Priority Research Program of Chinese Academy of Sciences (Grant XDA19060503), and the National Natural Science Foundation of China (Grant No. 42075002).

Data availability The hourly precipitation data can be downloaded from http://data.cma.cn/ with approval of China Meteorological Administration. The ERA5 dataset can be downloaded freely from https://cds.climate.copernicus.eu/cdsapp#!/home. The TC best-track dataset can be downloaded freely from https://tcdata.typhoon.org.cn/zjljsjj_zlhq.html.

Declarations

Conflict of interest The authors have no relevant financial or non-financial interests to disclose.

References

Bai L, Meng Z, Huang Y et al (2019) Convection initiation resulting from the interaction between a quasi-stationary dryline and intersecting gust fronts: a case study. J Geophys Res Atmos 124:2379–2396. https://doi.org/10.1029/2018JD029832

Bannon PR, Mak M (1984) Diabatic quasi-geostrophic surface frontogenesis. J Atmos Sci 41(14):2189–2201. https://doi.org/10.1175/1520-0469(1984)041%3c2189:DQGSF%3e2.0.CO;2

Blair D (1998) The Kirchhofer technique of synoptic typing revisited. Int J Climatol 18:1625–1635. https://doi.org/10.1002/(SICI)1097-0088(19981130)18:14%3c1625::AID-JOC330%3e3.0.CO;2-B

Cartwright TJ, Ray PS (1999) Radar-derived estimates of latent heating in the subtropics. Mon Weather Rev 127(5):726–742. https://doi.org/10.1175/1520-0493(1999)127%3c0726:RDEOLH%3e2.0.CO;2

Chen Y (2018) Multiple-scale characteristics of the extreme rainfall over South China during the presummer rainy season: Statistic analysis and a case study. PhD dissertation (in Chinese). University of Chinese Academy of Sciences

Chen GTJ, Wang CC, Wang AH (2007) A case study of subtropical frontogenesis during a blocking event. Mon Weather Rev 135(7):2588–2609. https://doi.org/10.1175/MWR3412.1

Chen X, Ding Z, Liu C et al (2012) Statistic analysis on the formation system of warm-sector heavy rainfall in May and June from 2000–2009. J Trop Meteorol 28:707–718. https://doi.org/10.3969/j.issn.1004-4965.2012.05.010. (**in Chinese**)

Chen Z, Lin W, Jiang B et al (2021) Effects of coastline and terrain on warm-sector heavy rainfall in the Pearl River Delta, South China. Acta Sci Nat Univ Sunyatseni. https://doi.org/10.13471/j.cnki.acta.snus.2021D012

Ding Y (1994) Monsoons over China. Springer, Netherlands, Dordrecht

Dong Y, Li J, Guo J et al (2020) The impact of synoptic patterns on summertime ozone pollution in the North China Plain. Sci Total Environ 735:139559. https://doi.org/10.1016/j.scitotenv.2020.139559

Du Y, Chen G (2018) Heavy rainfall associated with double low-level jets over Southern China. Part I: ensemble-based analysis. Mon Weather Rev 146:3827–3844. https://doi.org/10.1175/MWR-D-18-0101.1

Du Y, Chen G (2019) Climatology of low-level jets and their impact on rainfall over Southern China during the early-summer rainy season. J Clim 32:8813–8833. https://doi.org/10.1175/JCLI-D-19-0306.1

Du Y, Zhang Q, Chen Y et al (2014) Numerical simulations of spatial distributions and diurnal variations of low-level jets in China during early summer. J Clim 27:5747–5767. https://doi.org/10.1175/JCLI-D-13-00571.1

Du Y, Shen Y, Chen G (2022) Influence of coastal marine boundary layer tets on rainfall in South China. Adv Atmos Sci 39(5):782–801. https://doi.org/10.1007/s00376-021-1195-7

Guan P, Chen G, Zeng W et al (2020) Corridors of Mei-Yu-season rainfall over eastern China. J Clim 33(7):2603–2626. https://doi.org/10.1175/JCLI-D-19-0649.1

Han H, Liu J, Yuan H et al (2018) Impacts of synoptic weather patterns and their persistency on free tropospheric carbon monoxide concentrations and outflow in eastern China. J Geophys Res Atmos 123:7024–7046. https://doi.org/10.1029/2017JD028172

He L, Chen T, Kong Q (2016) A review of studies on prefrontal torrential rain in South China. J Appl Meteor Sci 27:559–569. https://doi.org/10.11898/1001-7313.20160505. (**in Chinese**)

Hersbach H, Bell B, Berrisford P et al (2020) The ERA5 global reanalysis. Q J R Meteorol Soc 146:1999–2049. https://doi.org/10.1002/qj.3803

Hoffmann P, Schlünzen KH (2013) Weather pattern classification to represent the urban heat island in present and future climate. J Appl Meteorol Climatol 52:2699–2714. https://doi.org/10.1175/JAMC-D-12-065.1

Huang S, Coauthors (1986) Rainstorms during Pre-rainy Season in South China. Guangdong Science and Technology Press, Guangzhou (**in Chinese**)

Huang X, Zhang C, Fei J et al (2022) Uplift mechanism of coastal extremely persistent heavy rainfall (EPHR): the key role of low-level jets and ageostrophic winds in the boundary layer. Geophys Res Lett 49:e2021GL096029. https://doi.org/10.1029/2021GL096029

Huangfu J, Huang R, Chen W (2017) Statistical analysis and a case study of tropical cyclones that trigger the onset of the South China Sea summer monsoon. Sci Rep 7:12732. https://doi.org/10.1038/s41598-017-13128-2

Huth R (1996) An intercomparison of computer-assisted circulation classification methods. Int J Climatol 16:893–922. https://doi.org/10.1016/j.pce.2009.11.013

Huth R, Beck C, Philipp A et al (2008) Classifications of atmospheric circulation patterns. Ann N Y Acad Sci 1146:105–152. https://doi.org/10.1196/annals.1446.019

Kajikawa Y, Wang B (2012) Interdecadal change of the South China Sea summer monsoon onset. J Clim 25:3207–3218. https://doi.org/10.1175/JCLI-D-11-00207.1

Li X, Du Y (2021) Statistical relationships between two types of heavy rainfall and low-level jets in South China. J Clim 34:8549–8566. https://doi.org/10.1175/JCLI-D-21-0121.1

Li D, Sun J, Fu S et al (2016) Spatiotemporal characteristics of hourly precipitation over central eastern China during the warm season of 1982–2012. Int J Climatol 36:3148–3160. https://doi.org/10.1002/joc.4543

Liang Z, Gao S (2021) Organized warm-sector rainfall in the coastal region of South China in an anticyclone synoptic situation: observational analysis. J Meteorol Res 35:460–477. https://doi.org/10.1007/s13351-021-0157-4

Liang Z, Fovell RG, Liu Y (2019) Observational analysis of the characteristics of the synoptic situation and evolution of the organized warm-sector rainfall in the coastal region of South China in the pre-Summer rainy season. Atmos 10:722. https://doi.org/10.3390/atmos10110722

Lin L (2006) Technical guidance on weather forecasting in Guangdong Province. China Meteorological Press, Beijing (**in Chinese**)

Lin Q, Shou S, Yang H (2015) Analysis on formation mechanism of the backflow rainstorm occurring in first rainy season of Guangxi based on numerical simulation. Meteor Mon 41:852–862. https://doi.org/10.7519/j.issn.1000-0526.2015.07.007. (**in Chinese**)

Lin Q, Zhao H, Lin B (2020) Comparative analysis on backflow warm-sector rainstorm cases in double rain belts process. J Trop Meteor 36:721–733. https://doi.org/10.16032/j.issn.1004-4965.2020.065. (**in Chinese**)

Liu N, Zhou S, Liu C et al (2019a) Synoptic circulation pattern and boundary layer structure associated with PM2.5 during wintertime haze pollution episodes in Shanghai. Atmos Res 228:186–195. https://doi.org/10.1016/j.atmosres.2019.06.001

Liu R, Sun J, Chen B (2019b) Selection and classification of warm-sector heavy rainfall events over South China. Chin J Atmos Sci 43:119–130. https://doi.org/10.3878/j.issn.1006-9895.1803.17245. (**in Chinese**)

Liu R, Sun J, Fu S (2021) Comparison of synoptic circulation characteristics in different types of warm-sector heavy rainfall events over South China. Climatic Environ Res 26:359–373. https://doi.org/10.3878/j.issn.1006-9585.2021.20105. (**in Chinese**)

Liu H, Huang X, Fei J et al (2022) Spatiotemporal features and associated synoptic patterns of extremely persistent heavy rainfall over China. J Geophys Res Atmos 127:e2022JD036604. https://doi.org/10.1029/2022JD036604

Lu X, Yu H, Ying M et al (2021) Western North Pacific tropical cyclone database created by the China meteorological administration. Adv Atmos Sci 38:690–699. https://doi.org/10.1007/s00376-020-0211-7

Luo M, Lin L (2017) Objective determination of the onset and withdrawal of the South China Sea summer monsoon: objective determination of monsoon onset and withdrawal. Atmos Sci Lett 18:276–282. https://doi.org/10.1002/asl.753

Luo Y, Wu M, Ren F et al (2016) Synoptic situations of extreme hourly precipitation over China. J Clim 29:8703–8719. https://doi.org/10.1175/JCLI-D-16-0057.1

Miao Y, Guo J, Liu S et al (2017) Classification of summertime synoptic patterns in Beijing and their associations with boundary layer structure affecting aerosol pollution. Atmos Chem Phys 17:3097–3110. https://doi.org/10.5194/acp-17-3097-2017

Ning G, Yim SHL, Yang Y et al (2020) Modulations of synoptic and climatic changes on ozone pollution and its health risks in mountain-basin areas. Atmos Environ 240:117808. https://doi.org/10.1016/j.atmosenv.2020.117808

Reeves HD, Lackmann GM (2004) An investigation of the influence of latent heat release on cold-frontal motion. Mon Weather Rev 132(12):2864–2881. https://doi.org/10.1175/MWR2827.1

Richman MB (1981) Obliquely rotated principal components: an improved meteorological map typing technique? J Appl Meteorol 20:1145–1159. https://doi.org/10.1175/1520-0450(1981)020%3c1145:ORPCAI%3e2.0.CO;2

Sun J, Wei J, Fu S et al (2018) The multi-scale physical model for persistent heavy rainfall events in the Yangtze-Huaihe River Valley. Chin J Atmos Sci 42:741–754. https://doi.org/10.3878/j.issn.1006-9895.1803.17246

Sun J, Zhang Y, Liu R et al (2019) A review of research on warm-sector heavy rainfall in China. Adv Atmos Sci 36:1299–1307. https://doi.org/10.1007/s00376-019-9021-1

Tang Y, Huang A, Wu P et al (2021) Drivers of summer extreme precipitation events over East China. Geophys Res Lett. https://doi.org/10.1029/2021GL093670

Wang D, Xia R, Liu Y (2011) A preliminary study of the flood-causing rainstorm during the first rainy season in South China. Acta Meteor Sinica 69:137–148. https://doi.org/10.11676/qxxb2011.012. (**in Chinese**)

Wang H, Sun J, Wei J et al (2014) Classification of persistent heavy rainfall events over southern China during recent 30 years. Clim Environ Res 19:713–725. https://doi.org/10.3878/j.issn.1006-9585.2013.13143. (**in Chinese**)

Wang H, Sun J, Zhao S et al (2016) The multiscale factors favorable for a persistent heavy rain event over Hainan Island in October 2010. J Meteorol Res 30:496–512. https://doi.org/10.1007/s13351-016-6005-2

Wang X, Zhou R, Deng Y et al (2022) Symbiotic relationship between mei-yu rainfall and the morphology of Mei-Yu Front. J of Hydrometeorol 23(1):87–100. https://doi.org/10.1175/JHM-D-21-0068.1

Wen W, Shen T, Ding Z et al (2010) Numerical experiment on the effect of urbanization upon summer land-sea breezes in the coastland of Guangxi. J Trop Meteorol 16(3):263–270. https://doi.org/10.3969/j.issn.1006-8775.2010.03.008

Wu N, Ding X, Wen Z et al (2020a) Contrasting frontal and warm-sector heavy rainfalls over South China during the early-summer rainy season. Atmospheric Res 235:104693. https://doi.org/10.1016/j.atmosres.2019.104693

Wu N, Wen Z, Den W et al (2020b) Advances in warm-sector heavy rainfall during the first rainy season in South China. J Meteorol Sci 40:605–616. https://doi.org/10.3969/2020jms.0077. (**in Chinese**)

Xia R, Zhao S, Sun J (2006) A study of circumstances of meso-β-scale systems of strong heavy rainfall in warm sector ahead of fronts in South China. Chin J Atmos Sci 30:988–1008 (**in Chinese**)

Xu J, Chang L, Ma J et al (2016) Objective synoptic weather classification on PM2.5 pollution during autumn and winter seasons in Shanghai. Acta Sci Circum 36:4303–4314. https://doi.org/10.13671/j.hjkxxb.2016.0224. (**in Chinese**)

Yang J, Zhao X, Tao Y et al (2021a) Characteristics of ozone weather in Chengdu during summer of 2016–2019. Res Environ Sci 34:254–262. https://doi.org/10.13198/j.issn.1001-6929.2020.10.20. (**in Chinese**)

Yang Y, Wang R, Chen F et al (2021b) Synoptic weather patterns modulate the frequency, type and vertical structure of summer precipitation over Eastern China: a perspective from GPM observations. Atmos Res 249:105342. https://doi.org/10.1016/j.atmosres.2020.105342

Ye L, Miao J (2014) Mesoscale analysis of a typical heavy rain event caused by returning flow in the warm sector in southern China. Torrential Rain Disaster 33:342–350. https://doi.org/10.3969/j.issn.1004-9045.2014.04.006. (**in Chinese**)

Ye L, Xu B (2014) Contrastive analysis of two different type rainstorms in warm area. J Meteorol Res Appl 35:5–10. https://doi.org/10.3969/j.issn.1673-8411.2014.04.002. (**in Chinese**)

Yin J, Zhang D-L, Luo Y et al (2020) On the extreme rainfall event of 7 May 2017 over the coastal city of Guangzhou. Part I: impacts of urbanization and orography. Mon Weather Rev 148:955–979. https://doi.org/10.1175/MWR-D-19-0212.1

Ying M, Zhang W, Yu H et al (2014) An overview of the China meteorological administration tropical cyclone database. J Atmos Ocean Technol 31:287–301. https://doi.org/10.1175/JTECH-D-12-00119.1

Zeng W, Chen G, Du Y et al (2019) Diurnal variations of low-level winds and precipitation response to large-scale circulations during a heavy rainfall event. Mon Weather Rev 147(11):3981–4004. https://doi.org/10.1175/MWR-D-19-0131.1

Zeng W, Chen G, Bai L et al (2022) Multiscale processes of heavy rainfall over East Asia in summer 2020: diurnal cycle in response to synoptic disturbances. Mon Weather Rev 150(6):1355–1376. https://doi.org/10.1175/MWR-D-21-0308.1

Zhang M, Meng Z (2019) Warm-sector heavy rainfall in southern China and its WRF simulation evaluation: a low-level-jet perspective. Mon Weather Rev 147:4461–4480. https://doi.org/10.1175/MWR-D-19-0110.1

Zhang C, Huang X, Fei J et al (2021a) Spatiotemporal characteristics and associated synoptic patterns of extremely persistent heavy rainfall in Southern China. J Geophys Res Atmos. https://doi.org/10.1029/2020JD033253

Zhang Y, Sun J, Zhu L et al (2021b) Comparison of two types of persistent heavy rainfall events during sixteen warm seasons in the Sichuan Basin. Atmos Ocean Sci Lett. https://doi.org/10.1016/j.aosl.2021.100094